Biomedical Signal Processing and Control 40 (2018) 117–130

Contents lists available at ScienceDirect

Biomedical Signal Processing and Control

journal homepage: www.elsevier.com/locate/bspc

Research paper

Computer aided thyroid nodule detection system using medical ultrasound images

Deepika Koundal [a,b,*], Savita Gupta [b], Sukhwinder Singh [b]

[a] Department of Computer Science & Engineering, Chitkara University Institute of Engineering & Technology, Chitkara University, India
[b] Department of Computer Science & Engineering, University Institute of Engineering & Technology, Panjab University, Chandigarh, India

ARTICLE INFO

Article history:
Received 22 October 2016
Received in revised form 31 July 2017
Accepted 24 August 2017

Keywords:
Neutrosophic
Graphical user interface
Computer aided detection
Speckle reduction
Image segmentation

ABSTRACT

Thyroid nodule is one of the endocrine problem caused due to abnormal growth of cells. This survival rate can be enhanced by earlier detection of nodules. Thus, the accurate detection of nodule is of utmost importance in providing effective diagnosis to increase the survival rate. However, accuracy of nodule detection from ultrasound images is suffered due to speckle noise. It considerably deteriorates the image quality and makes the differentiation of fine details quite difficult. Most of the detection systems for the thyroid nodules are semi-automated entailing manual intervention to draw rough outline of the nodule at some level or require manual segmentation in training or testing phases that increase the inaccuracies and evaluation time. To handle this, a fully Computer-Aided Detection system is presented for speckle reduction and segmentation of nodules from thyroid ultrasound images. The proposed system has three components: speckle reduction to reduce speckle noise and preserve the diagnostic features of ultrasound image, automatic generation of Region of interest (ROI) that identifies suspicious regions and fully automatic segmentation of nodule in processed ROI image. The proposed segmentation method outperformed other methods by gaining high True Positive (TP) value ($95.92 \pm 3.70\%$), False Positive (FP) value ($7.04 \pm 4.21\%$), Dice Coefficient (DC) value ($93.88 \pm 2.59\%$), Overlap Metric (OM) (91.18 ± 7.04 pixels) and Hausdroff Distance (HD) (0.52 ± 0.20 pixels). This system can facilitate the endocrinologists by providing second opinion to improve diagnosis of nodules as benign or malignant.

1. Introduction

Nodule is the abnormal growth of cells (lumps) within the thyroid gland that may be benign (non-cancerous) or malignant (cancerous) [1,2]. In general, the occurrence of thyroid nodule among all the cancer cases is reported to be around 0.2% [34,30,37,29]. The prevalence of this type of cancer increases with the age and is one of the most common cancers among women [3]. According to American Cancer Society's estimates for thyroid cancer, out of 62,450 new cases of thyroid cancer, 6.7% were males and 20% were females and 1950 (1080 women and 870 men) estimated deaths were expected due to thyroid cancer for 2015 in United States [42]. As per these medical statistics, thyroid nodule is a severe disorder leading to high mortality rate. However, the mortality rate can be reduced if cases are detected and treated early by finding the initial symptoms of thyroid nodule [14].

Ultrasound is used as the most common imaging modality for early thyroid nodules detection. It is generally preferred due to its non-ionising radiation effects, inexpensive and painless scanning operations which provide diagnostically important information needed for medical diagnosis [22]. However, the key challenge in automated analysis in ultrasound images is to make accurate nodules segmentation within the thyroid gland. As these images are affected by speckle noise and intensity in-homogeneity that may appear as bright spots. Speckle noise can be described as a texture pattern that changes with the type of biological tissue. It deteriorates the image quality and makes the differentiation of fine details difficult. The major purpose of speckle reduction is to improve the image quality [19,15] for accurate segmentation of nodules. However, the removal of speckle noise is always a trade-off between edge preservation and noise suppression.

Doctors interpret the ultrasound images to provide effective treatment in order to identify the severity of several thyroid diseases. Occasionally, practitioners make perception and interpretation errors while performing the diagnosis [20]. Perception errors occur when anomalies remain undetected even when it is in sight and interpretation errors occur when a detected abnormality is incorrectly interpreted as benign or malignant. These errors can

* Corresponding author at: Department of Computer Science & Engineering, Chitkara University Institute of Engineering & Technology, Chitkara University, India.
E-mail addresses: deepika.koundal@chitkara.edu.in (D. Koundal), savita2k8@gmail.com (S. Gupta), sukhdalip@pu.ac.in (S. Singh).

http://dx.doi.org/10.1016/j.bspc.2017.08.025
1746-8094/

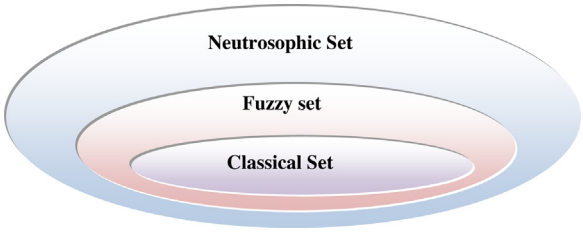

Fig. 1. Relationship among classical set, fuzzy set and neutrosophic set [39].

be due to distractions, endocrinologist exhaustions, Human Visual System (HVS) limitations and experience level. This uncertainty can be finally resolved by invasive procedures such as biopsies and Fine Needle Aspiration (FNA). The critical issue for an endocrinologist is to manually detect the accurate thyroid nodule in the ultrasound image and classify it as benign or malignant [16]. Therefore, Computer assisted detection systems are becoming popular which assist endocrinologists in accurate decision making for interpretation of huge amount of image data [22]. One of the key challenges to be considered in the design of fully Computer-Aided Detection system is to make accurate delineation of nodules with automatic extraction of Region of Interest (ROI) within the thyroid gland. The other challenges are speckle noise suppression in ultrasound images in some intuitive ways so that indeterminacy and fuzziness can be easily handled without using any prior information and human intervention. The goal is to preserve texture details which have high degree of indeterminacy due to resemblance to the speckle noise.

Fuzzy domain is most widely used by the researchers for handling fuzziness [7]. Fuzzy set (FS) is widely used in image processing applications [4]. FS can only deal with the membership degree but is not able to handle the indeterminacy degree of uncertain pixels [44–46]. Unlike fuzzy logic, neutrosophic logic introduces the extra domain *IM* that provides a more efficient way to handle higher degrees of indeterminacy that are very difficult to be handled by fuzzy logic. The relationship among classical set, fuzzy set and neutrosophic set is shown in Fig. 1. In case of classical set, *TM* and *FM* have either 0 or 1 values and $IM = \emptyset$. While in fuzzy set, $IM = \emptyset$ but *TM* and *FM* are real numbers $\in$ [0,1] and sum of *TM* and *FM* must be equal to 1. In neutrosophic set, there is no limit on the sum of *TM*, *IM* and *FM* that is *TM*, *IM*, *FM* $\in .]^{-}0,1^{+}[$. Statistically, *TM*, *IM* and *FM* are the membership subsets which depend on known and unknown aspects.

Recently, generalization of fuzzy set named as Neutrosophic Set (NS) is becoming popular in image processing applications [8,19,20,38,9,31,39,18]. Many researchers have used Neutrosophy in variety of applications like image denoising and segmentation which have shown that neutrosophic based methods yield good performance due to their indeterminacy handling capability [38,8,10,18]. Thus, this paper presented a Computer Aided Detection (CADe) system using neutrosophic based speckle removal method and segmentation method that can provide another opinion to endocrinologists for accurate nodule detection and reduction of unnecessary invasive biopsy operations and surgical complications.

The rest of paper is structured as: Section 2 discusses material and Computer aided detection system with speckle reduction and segmentation of thyroid nodules. Section 3 discusses the experiments and results while section 4 gives conclusion.

2. Material and methods

2.1. Material

2.1.1. Dataset

In this paper, two real ultrasound image datasets have been used to validate the efficacy of speckle reduction and segmentation methods. The first dataset of real thyroid ultrasound images is acquired from the Department of Radiology, Post Graduate Institute of Medical Education & Research, Chandigarh, India. It consists of 50 subjects, out of which, 20 were males and 30 were females, age from 15 to 70 years. The images were acquired with a 256 grey-level depth using IU22 Philips X Matrix with linear probe at a frequency of 17.5 MHz having 628×656 pixels. Each nodule is delineated by expert and the manual segmentation is served as ground truth for making comparison. The second dataset is obtained from open access Digital Database of Thyroid ultrasound Images (DDTI) from the website of Computer Imaging & Medical Applications Laboratory, Universidad Nacional de Colombia [36]. This dataset consists of 88 thyroid ultrasound images.

2.1.2. Performance measures

To investigate the performance of segmentation methods both area-based and boundary-based metrics have been used in this work. Area based error metrics such as True Positive (TP), False Positive (FP), Overlap Metric (OM) and Dice Coefficient (DC) are used to compute the number of pixels covered by the automated method correctly and wrongly. The boundary based error metrics such as Hausdroff Distance (HD) and Mean Absolute Distance (MAD) are used to determine the possible disagreement over two curves [6,43].

2.2. Methods

2.2.1. Neutrosophy

Smarandache introduced Neutrosophy to handle nature and scope of neutralities [40,41,17]. Neutrosophic theory gives a general framework to handle indeterminacy. Many researchers have explored several applications such as image de-noising and image segmentation. It generalizes fuzzy logic and handles the antitheses, antinomies, contradictions and paradoxes. The term '*Neutrosophy*', has appeared from the Latin term '*Neuter*' as neutral and Greek term '*Sophia*' as skill/wisdom [31,39]. Neutrosophy theory takes into account every concept, entity, or event $\langle A \rangle$ associated to its converse $\langle Anti\text{–}A \rangle$, the neutralities $\langle Neut\text{–}A \rangle$ and which is not A $\langle Non\text{–}A \rangle$ [39]. The three membership subsets are used to determine the truth degree, indeterminacy degree and falsity degree of $\langle A \rangle$.

Neutrosophic Set (NS) considers the nature, scope and origin of neutralities. In neutrosophic logic, three neutrosophic components: True Membership (*TM*), Indeterminate Membership (*IM*) and False Membership (*FM*) are defined to estimate the degree of truth, the degree of indeterminacy (neither true nor false) and the degree of falsity [40,41,17].

2.2.1.1. Neutrosophic image. An image in neutrosophic domain P_{NI} is considered as *TM*, *IM* and *FM* subsets [39]. A pixel in neutrosophic domain can be characterized as $P_{NI}\left\{t_m, i_m, f_m\right\}$, representing the pixel as t_m% true (nodule), i_m% indeterminate (nodule boundaries) and f_m% false (background), where $t_m TM \in$, $i_m IM \in$, and $f_m \in FM$ [32,33].

2.2.2. Proposed computer aided thyroid nodule detection system

Fig. 2 illustrates the block diagram of the proposed Computer-Aided Detection (CADe) system for thyroid nodules. The proposed CADe system consists of following phases: Speckle reduction, Region of Interest (ROI) extraction [24] and thyroid nodule segmentation. Firstly, speckle reduction method named as Neutrosophic Nakagami Total Variation (NNTV) is applied to remove speckle noise, then ROI is extracted automatically and finally proposed Neutrosophic Distance Regularized Level Set (NDRLS) method has been utilized for the segmentation of thyroid nodules.

Fig. 2. The block diagram of the proposed Computer-Aided Detection (CADe) system.

2.2.2.1. Speckle reduction method. The speckle reduction method firstly transform the image into neutrosophic domain. Secondly, neutrosophic entropy is computed to handle indeterminacy and neutrosophic based filtering operation is applied for speckle reduction. Lastly, image is converted into gray level domain from neutrosophic domain.

In neutrosophic domain *TM*, *IM* and *FM* are the neutrosophic components used to denote <*A*>, <*Neut-A*> and <*Anti-A*> respectively.

Every neutrosophic image pixel can be denoted as $P_{NI} = \{TM, IM, FM\}$, where *TM*, *IM* and *FM* are the pixels probabilities that belong to the white pixels set, indeterminate pixels set and non-white pixels set respectively [32]. The membership functions *TM*, *IM* and *FM* are computed to transform image from gray level domain to neutrosophic domain. The membership functions *TM*, *IM* and *FM* are computed [33] as given below:

$$TM = \frac{\hat{f}_{ij} - \hat{f}_{min}}{\hat{f}_{max}} \tag{1}$$

where i varies from 0 to n-1, j varies from 0 to m-1, $\hat{f}_{ij}$ is the local mean obtained using window, $\hat{f}_{min}$ is the minimum gray level value and $\hat{f}_{max}$ is the maximum gray level value.

$$\hat{f}_{ij} = \frac{1}{w \times w} \sum_{m=i-\frac{w}{2}}^{i+\frac{w}{2}} \sum_{n=j-\frac{w}{2}}^{j+\frac{w}{2}} f_{mn} \tag{2}$$

where f_{mn} is the noisy image, $\hat{f}_{ij}$ is the pixel's local mean on a window and w is the size of window .

$$IM = \frac{\delta_{ij} - \delta_{min}}{\delta_{max}} \tag{3}$$

$$\delta_{ij} = abs\left(f_{ij} - \hat{f}_{ij}\right) \tag{4}$$

where δ_{ij} is the absolute difference between intensity f_{ij} and its local mean value $\hat{f}_{ij}$, $\delta_{\min}$ is the minimum value of absolute difference and $\delta_{\max}$ is the maximum value of absolute difference. The false membership in neutrosophic domain is computed as

$$FM = 1 - TM \tag{5}$$

The true subset, *TM*, in neutrosophic domain is processed by normalizing the gray levels in [0, 1] as given in Eq. (1). In ultrasound images, pixels belonging to speckle and texture are hard to differentiate, therefore, neighbourhood mean, $\hat{f}_{ij}$, is applied to determine the local mean of pixels on a window. The absolute difference, δ_{ij}, between intensity value, f_{ij}, and its local mean value, $\hat{f}_{ij}$, is computed to determine the indeterminate image component. False subset, *FM*, is computed as the complement of *TM*.

The indeterminate pixels are measured by *TM* values after the transformation of image into the neutrosophic domain [33]. The correlation of *TM* with *IM* varies with the distribution of pixels in *IM* and consequently modifies the entropy of *IM*. A neutrosophic filtering operation for pixel $P(NI)$ is represented as

$$P(NI) = P(TM, IM)) \tag{6}$$

where $P(NI)$ is the pixel value in neutrosophic image, *TM* is the true membership component in neutrosophic image and *IM* is the indeterminate membership subset in neutrosophic image.

In this work, Nakagami Total Variation (NTV) [23] is explored in Neutrosophic domain for filtering operation (NNTV) [25,26], which can be represented as

$$TM = arg \min_{TM} \left\{ \sum_{\substack{1 \le i \le m, \\ 1 \le j \le n}} (2TM + \frac{1}{2\sigma^2} e^{2(x-TM)}) + \lambda \|\nabla TM\|_2 \right\} \tag{7}$$

The details of solving NTV is given in [25]. Take this line above.The pixels of *TM* component are processed on the basis of *IM* represented as

$$TM = \begin{cases} TM & IM < \chi \\ TM & IM \ge \chi \end{cases} \tag{8}$$

where χ is the indeterminacy threshold. The value of χ is used to control the indeterminacy of image and is set to 1.2 by checking the optimal value at step interval of 0.1 from 0 to 10. If *IM* value is less than χ then no filtering will be applied on *TM*, else, variational filtering operation *TM* will be employed (based on nakagami statistics).

$$IM = \frac{\delta_{TM} - \delta_{TM_{min}}}{\delta_{TM_{max}}} \tag{9}$$

$$\delta_{TM} = abs(TM - TM) \tag{10}$$

where δ_{TM} is the absolute difference between filtering operation *TM* and *TM* after χ operation.

After speckle reduction, finally neutrosophic image is transformed to gray level domain from neutrosophic domain by Eq. (11).

$$\hat{\hat{f}} = \hat{f}_{min} + \left(\hat{f}_{max} + \hat{f}_{min}\right) \cdot \hat{T\hat{M}} \tag{11}$$

where $\hat{f}_{min}$ is the minimum intensity value, $\hat{f}_{max}$ is the maximum intensity value and $\hat{T\hat{M}}$ component is processed based on *IM* after applying neutrosophic variational filtering operation. The Neutrosophic Domain Speckle Reduction method can be implemented using Algorithm 1.

Algorithm 1: Neutrosophic Domain Speckle Reduction Method

INPUT: Noisy image, f.

OUTPUT: Speckle suppressed image, $\hat{\hat{f}}$.

Set epsilon $(\varepsilon) = 1e-4$, iteration index $(k) = 0$.

Step 1: Transform image into neutrosophic domain [32]

Step 2: Perform filtering operation to obtain $\widehat{TM}$ and $\widehat{IM}$.

Step 3: Compute entropy of the indeterminate subset $\widehat{IM}$ to obtain entropy $En_{IM}(k)$.

Step 4: If

$$\frac{En_{IM}(k+1) - En_{IM}(k)}{En_{IM}(k)} < \varepsilon,$$

Goto Step 5; else $TM = \widehat{TM}$ and $IM = \widehat{IM}$ goto Step 2.

Step 5: Transform $\widehat{\widehat{TM}}$ to the gray level domain from neutrosophic domain.

2.2.2.2. Segmentation method. Distance Regularized Level Set Evolution (DRLSE) and Neutrosophic L-Means (NLM) clustering are the most common methods used for image segmentation.

2.2.2.3. Distance regularized level set evolution (DRLSE). Osher and Sethian presented the level set for curve evolution in 1988 [35]. Generally, Level set methods often used re-initialization as a mathematical solution for consistent results and curve evolution. But re-initialization leads to high computational cost which can be overcome by utilizing DRLSE [27]. Therfore, it avoids the re-initialization problem and reduces the computational cost.

Let $\varphi : \Omega \rightarrow \Re$ be a Level Set Function (LSF) expressed on image domain Ω. The gradient flow of energy function $\varepsilon ng(\varphi)$ can be depicted as

$$\varepsilon ng(\varphi) = \mu \mathcal{R}eg_p(\varphi) + En_{ext}\left(g_{edge}, \varphi\right) \tag{12}$$

where $\mathcal{R}eg_p(\varphi)$ is the distance regularized term, $\mu > 0$ is a controlling parameter, g_{edge} is an edge indicator function and En_{ext} is the external energy term [27].

LSF may be initialized from binary region represented as

$$\varphi_0(x,y) = \begin{cases} -B_r & if \quad \varphi_0(x,y) \in \Omega_0 \\ B_r & otherwise \end{cases} \tag{13}$$

where Ω_0 is a subsetin Ω and 0 is a constant.

The main drawback of DRLSE is that it is influenced by the initial position of manually provided contour. Generally, the segmentation outcome is based on the shape and initial position of initial level set function. If the preliminary position of LSF is located far from the nodule, then LSF is likely to be kept at the periphery instead on the nodule. Thus, adequate initialization of level set function around the boundary of object is necessary for accurate segmentation.

2.2.2.4. Neutrosophic L-Means (NLM) clustering. Neutrosophic L-Means (NLM) Clustering is based on neutrosophy and Fuzzy C-Means (FCM) to group pixels into a lesion region and background [11]. Shan et al. presented a NLM clustering method for image segmentation based on FCM clustering [39]. The objective function of Neutrosophic L-Means (NLM) clustering can be represented using Eq. (14).

$$J_m^{NLM} = \sum_{i=1}^{N}\sum_{j=1}^{l} \mu_{ij}^m \| VT(1-VI) - l_j \|_{NLM}^2, \quad 1 \le m \le \infty \tag{14}$$

where m is exponential fuzziness, VT is the vector of true membership degree, VI is the vector of indeterminate membership degree, μ_{ij} is the membership degree, l_j is the cluster center and $||.||$ is any norm expressing the correspondence between any measured data and the cluster j.

The partitioning in neutrosophic domain is performed through iterative optimization of objective function given in Eq. (14), with the membership function u_{xy} and cluster center l_y by Eq. (15) and Eq. (16) respectively.

$$u_{xy} = \frac{1}{\sum_{d=1}^{L}\left(\frac{\|VT_x - l_y\|}{\|VT_x - l_d\|}\right)^{\frac{2}{m-1}}} \tag{15}$$

where L is number of clusters, $U^{(k)} = \left[u_{xy}\right]$ is the membership matrix, y is the cluster index and x is the pixel index.

$$l_y = \frac{\sum_{x=1}^{N} u_{xy}^m (1 - VI_x) VT}{\sum_{x=1}^{N} u_{xy}^m (1 - VI_x)} \tag{16}$$

where VT is transformed true vector, VI is transformed indeterminate vector and N is sum of entire pixels in image. If a pixel's indeterminate value is high, its contribution to all cluster centers is reduced, otherwise, its contribution to cluster centers is decided by its membership function.

Update image f_{ij}^{k+1} by

$$f_{ij}^{k+1} = \begin{cases} f_{ij}^{k} & if \quad IM^{(k)} < \lambda_{I\_T} \\ \hat{f}_{ij}^{k} & if \quad IM^{(k)} \ge \lambda_{I\_T} \end{cases} \tag{17}$$

where λ_{I_T} is the indeterminacy threshold value. In order to choose an optimum value of indeterminacy threshold, λ_{I_T}, different values from 0.1-step interval [0.1, 2.0] are taken for different type of images. This threshold value is used to distinguish high and low indeterminacy.

The iteration will stop when

$$\max_{ij}\left\{|U_{ij}^{(k+1)} - U_{ij}^{(k)}|\right\} < \varepsilon ps \tag{18}$$

where εps is a predefined stopping criterion between 0 and 1.

The output binary image, O_k, is obtained by:

$$O_k = \begin{cases} 1 & u_{x0} > u_{x1} \\ 0 & otherwise \end{cases} \tag{19}$$

where u_{x1} is the background membership function and u_{x0} is the foreground membership function.

2.2.2.5. Proposed segmentation method. This paper presents the new Neutrosophic based Distance Regularizer Level Set (NDRLS) method for automated segmentation of nodules in thyroid ultrasound images. The proposed method used the image intensity as

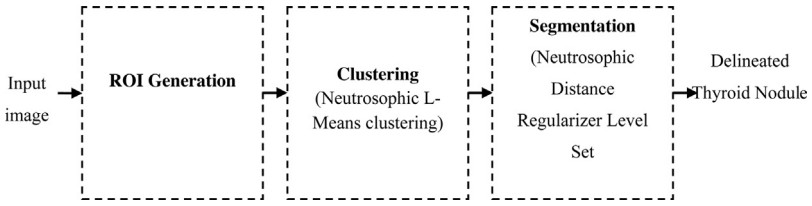

Fig. 3. Block diagram of proposed automated Neutrosophic Distance Regularizer Level Set.

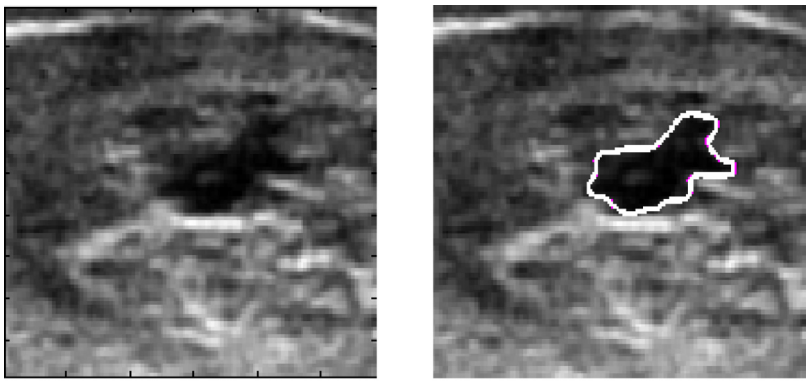

Fig. 4. Thyroid ultrasound (img7) **(a)** Original image. Segmentation results by **(b)** Proposed NDRLS method.

the main feature. The block diagram of fully automated segmentation system is shown in Fig. 3.

The proposed method is comprised of NLM clustering and NDRLS with adapted parameters. Initially, ROI extraction method is used to extract small rectangular region to remove the redundant background for facilitating full automation of image segmentation [24]. Subsequently, Neutrosophic L-Means (NLM) clustering provides the controlling parameters directly to the NDRLS. Finally, the NDRLS guided by NLM is presented to automatically segment the nodules. The NDRLS segmentation method incorporates NLM with level set to solve the manual initialization problem of level set. Therefore, in order to make fully automatic segmentation method, the proposed method requires approximation of the contours of nodule region from NLM clustering to initialize and regularize the level set as well as to estimate the various controlling parameters automatically. The proposed NDRLS method automates the initialization of level set using NLM and parameter configuration. The initial curve (LSF) will evolve firmly to the precise boundary of nodule with directly integration of NLM results. The object O_k obtained by NLM is close to the object of interest that is required to be segmented. Therefore, few iterative steps are required to push/pull the zero level set from O_k to the required curve.

The initial level set function φ_0^{NLM} obtained from NLM is employed to approximate actual boundaries. The NDRLS can be initialized from object of interest (O_k) as

$$\varphi_0^{NLM} = -\varepsilon\left(G\left(O_k\right)\right) \tag{20}$$

where ε is the dirac regulator for image smoothening and $G(O_k)$ is enhanced balloon force to push/pull the contour adaptively towards the O_k [28].

$$G\left(O_k\right) = 1 - 2(O_k) \tag{21}$$

There are several parameters required for DRLSE for image segmentation. In literature, certain rules are used for setting of optimum values of controlling parameters. As setting of higher value of α not only smoothens the image but also loses some details of image. The balloon force αinfluences the curve evolution direction. If the initial φ is outside the O_k then it is necessary to choose positive sign of α for shrinkage and vice-versa. The higher value of timestep τ may lead to problem of boundary leakage. From experimental results, it is observed that the higher values of α and λ_S accelerates the level set evolution and smoothens the contour respectively. But these rules are insufficient for optimum configuration of parameters in thyroid ultrasound image. Thus, it is essential to adjust these parameters automatically by NLM as given below.

Given the initial LSF φ_0^{NLM} from NLM, time step parameter τ can be computed as

$$\tau = \alpha / \ell \tag{22}$$

where ℓ is the length and α is the weighted area of initial LSF φ_0^{NLM} got from NLM clustering.

Thus, τ is calculated as

$$\tau = \frac{\int_\Omega g_{edge} H\left(\varphi_0^{NLM}\right) dxdy}{\int_\Omega g_{edge} \delta_\varepsilon\left(\varphi_0^{NLM}\right) dxdy} \tag{23}$$

Where, $\delta_\varepsilon\left(\varphi_0^{NLM}\right)$ is the dirac regulator function and $H\left(\varphi_0^{NLM}\right)$ is the Heaviside function.

The product of $\mu * \tau$ should be smaller than one-fourth for accurate evolution and stability [28]. The μ is computed as

$$\mu = \frac{0.2}{\tau} \tag{24}$$

The parameter λ_S controls the topological variations and prevents the leakage problem. For obtaining the smooth curve, weighting coefficient of contour length is calculated as

$$\lambda_S = 0.1 * \tau \tag{25}$$

Generally, in level set, balloon force $\alpha$is chosen as a global constant for different types of images. A larger value of αmay resulted in boundary leakage due to weak edges. To deal these issues, an enhanced $\alpha$is used in this work. Here, α is the weighted area got from initial LSF φ_0^{NLM} that is used to push/pull the contour adaptively towards O_k. The LSF pull towards O_k regardless of its initial location. From experiments, it has been observed that initial NLM

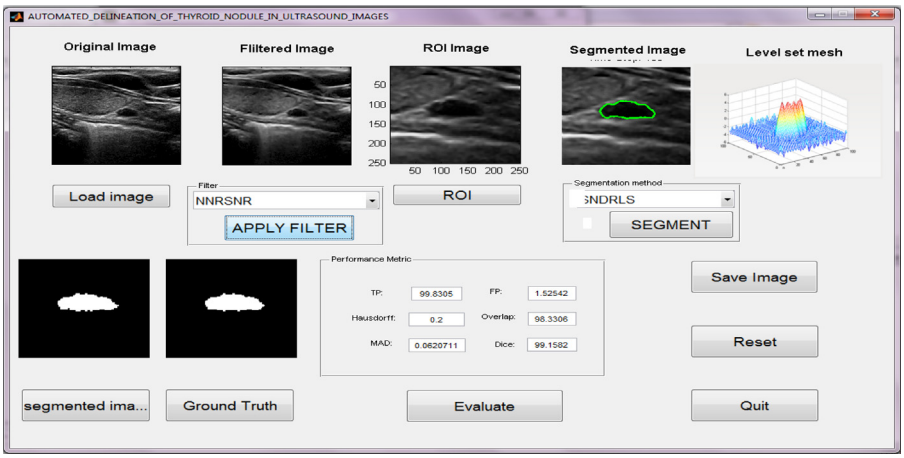

Fig. 5. View of segmentation and evaluation phases.

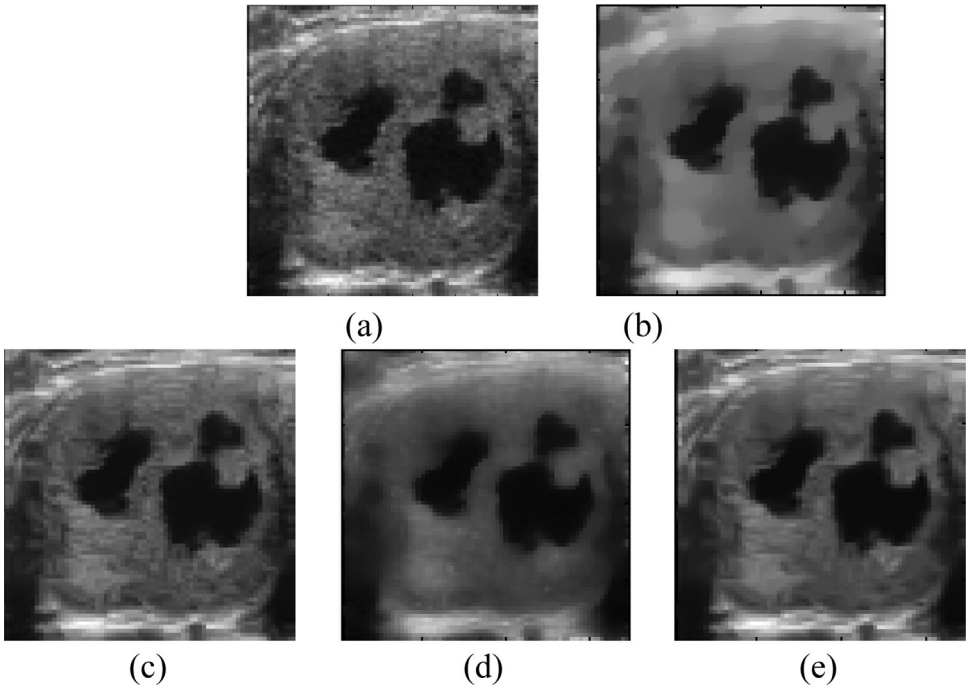

Fig. 6. Comparison of different speckle reduction methods on real image (img2) σ=0.5. **(a)** Original image **(b)** NRSNR **(c)** NNRSNR **(d)** NTV **(e)** NNTV.

can be considered as an index for curve evolution. The NDRLS obtain membership degree of each pixel u_{xy} as distance to the particular object O_k. Thus, external energy can be denoted as

$$En_{ext}(g,\varphi) = \lambda_S \delta_\varepsilon(\varphi)\, div\left(g_{edge}\frac{\nabla\varphi}{|\nabla\varphi|}\right) + G(O_k)\, g_{edge}\delta_\varepsilon(\varphi) \tag{26}$$

The evolving equation for NDRLS is represented as

$$\varphi^{k+1}(x,y) = \varphi^k(x,y) + \tau[\mu[\nabla^2\varphi - div(\frac{\nabla\varphi}{|\nabla\varphi|})]$$

$$+\delta_\varepsilon(\varphi) div(g_{edge}\frac{\nabla\varphi}{|\nabla\varphi|}) + (1-2(O_k))g_{edge}\delta_\varepsilon(\varphi)] \tag{27}$$

where k is the iteration index, τ is time step, λ_S is the weighting coefficient of contour length, μ is the regularization term weighting coefficient, O_k is an object obtained by NLM clustering, g_{edge} is an edge indicator function and δ_ε is the dirac delta function. The NDRLS initialization by NLM is fully automatic. The NLM is employed to derive the balloon force α directly. The evolution will automatically slow down as it move towards O_k. NDRLS become stable automatically with the assumption of conventional λ_S. These modifications avoid the excessive or inadequate segmentation. The proposed NDRLS method is given in Algorithm 2.

Further, the visual results of NLM clustering and proposed NDRLS methods are illustrated in Fig. 4. Original ultrasound image is shown in Fig. 4(a). Fig. 4(b) illustrates the delineated nodule boundary in thyroid ultrasound image using NDRLS method. The contour contracts, expands, merges or splits and pauses at the required position during NDRLS evolution for accurate delineation. It is also observed that NDRLS in neutrosophic domain has an ability to delineate the nodule accurately without any human intervention.

Algorithm 2. Proposed NDRLS method

Input: Approximated object of interest from NLM clustering.

Output: Segmented nodule

Step 1: Initialize LSF with NLM clustering and estimate parameters such as μ, τ, ε, λ_S, and α.

Step 2: Approximate ℓ and α of initial LSF φ_0^{NLM} using Eq. (22).

Step 3: Calculate τ and μ by Eq. (23) and Eq. (24) respectively.

Step 4: Step 4: Calculate λ_S by Eq. (25).

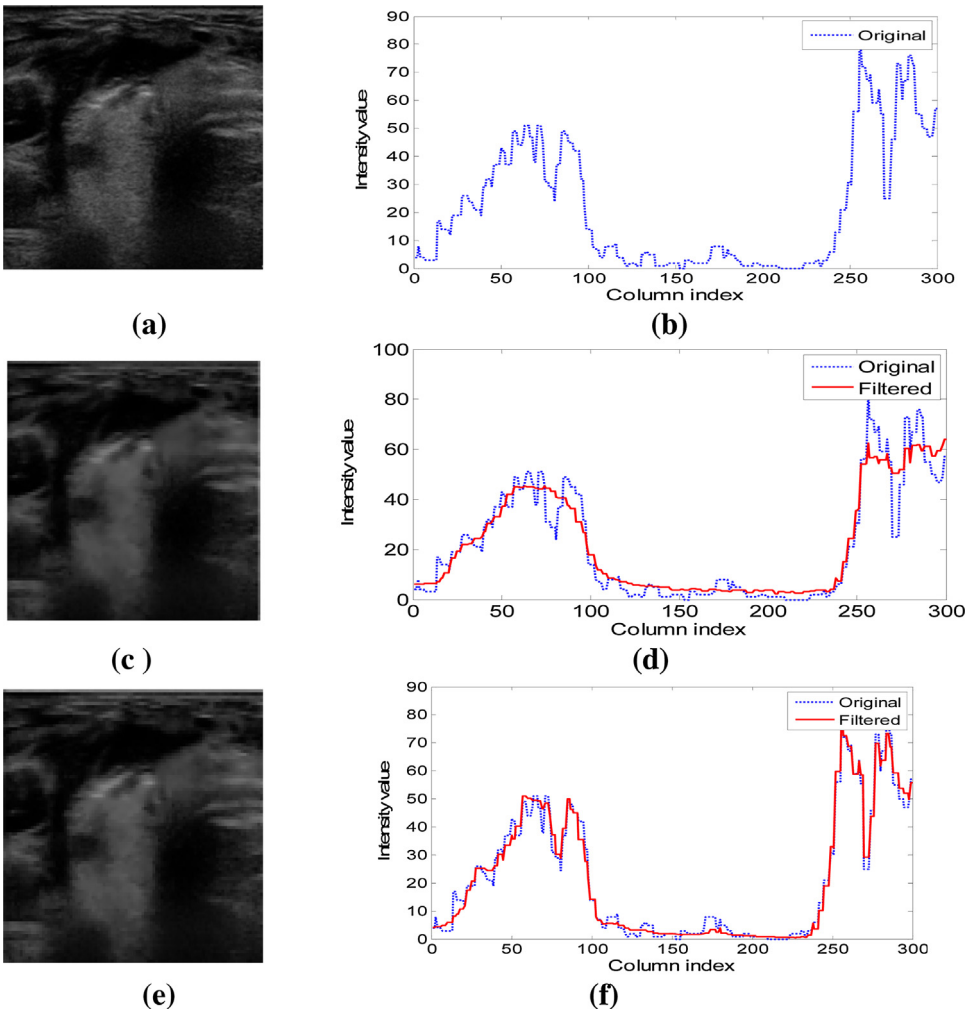

Fig. 7. Denoising results on the thyroid ultrasound image (img8) **(a)** Original image **(b)** Line profile of original image **(c)** NNRSNR **(d)** Line profile of NNRSNR **(e)** NNTV **(f)** Line profile of NNTV.

Step 5: Apply NDRLS for curve evolution using Eq. (27).

Subsequently, the last component is automatic segmentation method for thyroid nodule segmentation in ultrasound images. In this, a fully automated Neutrosophic based Distance Regularizer Level Set (NDRLS) method is proposed for accurate and effective segmentation. It integrated the Neutrosophic L-Means (NLM) clustering with DRLSE to solve the manual initialization problem by providing automatic initialization of the level set. In this work, the NLM clustering approximated the contours of nodule region for initializing and regularizing the level set function. Also, the NDRLS estimated the various controlling parameters adaptively from NLM and became stable as the implicit interface approaches the specific contours.

3. Graphical user interface of CADe system

Further, a Graphical User Interface (GUI) has been developed to incorporate the sequence of steps required for the segmentation of thyroid nodule into a single visual environment to let an easier handling of input images and saving of results. Fig. 5 illustrates a displaying of evaluation phase with segmentation phase. Initially, an image is selected and the result of each routine is displayed in the separate figure window such as filtered image, ROI extraction and segmentation. In **segmentation phase**, the "Load image" button is used for loading image. The "Apply filter" button includes menu to call speckle reduction methods such as Neutrosophic LEE (NLEE) [21], Neutrosophic KUAN (NKUAN) [21], Neutrosophic Nakagami Total Variation (NNTV) [26], Nakagami Total Variation (NTV) [23], Neutrosophic Nonconvex Regularizer Speckle Noise Removal (NNRSNR) [25] and Nonconvex Regularizer based Speckle Noise Removal NRSNR [13]. The user can select any method for the removal of speckle noise from ultrasound images. "ROI" button consists of a method for automatic extraction of ROI from a real ultrasound image. Then "Segmentation Method" button consists of menu to call segmentation methods namely Neutrosophic-L Means (NLM) [39], Neutrosophic C-Means (NCM) [12], Neutrosophic Watershed (NW) [44] and Proposed Neutrosophic Distance Regularized Level Set (NDRLS), along with figure window to display level set mesh. **Evaluation phase** consists of segmented and ground truth image along with performance metrics. "Evaluate" button is used for displaying the values of quality metrics to compare the performance of chosen computerized and manually segmented image. In addition, an option to save, reset and quit is provided.

All these functionalities have been integrated into a simple and user-friendly GUI environment designed for ease of application. For the segmentation of thyroid nodules in ultrasound image, high accuracy entails more manual involvement and achieving complete computerization is often at the cost of precision. The proposed CADe system effectively solves such problems. It is completely automatic and achieves accurate segmentation. Therefore, CADe system can be further used for computer-aided diagnosis of thyroid nodules.

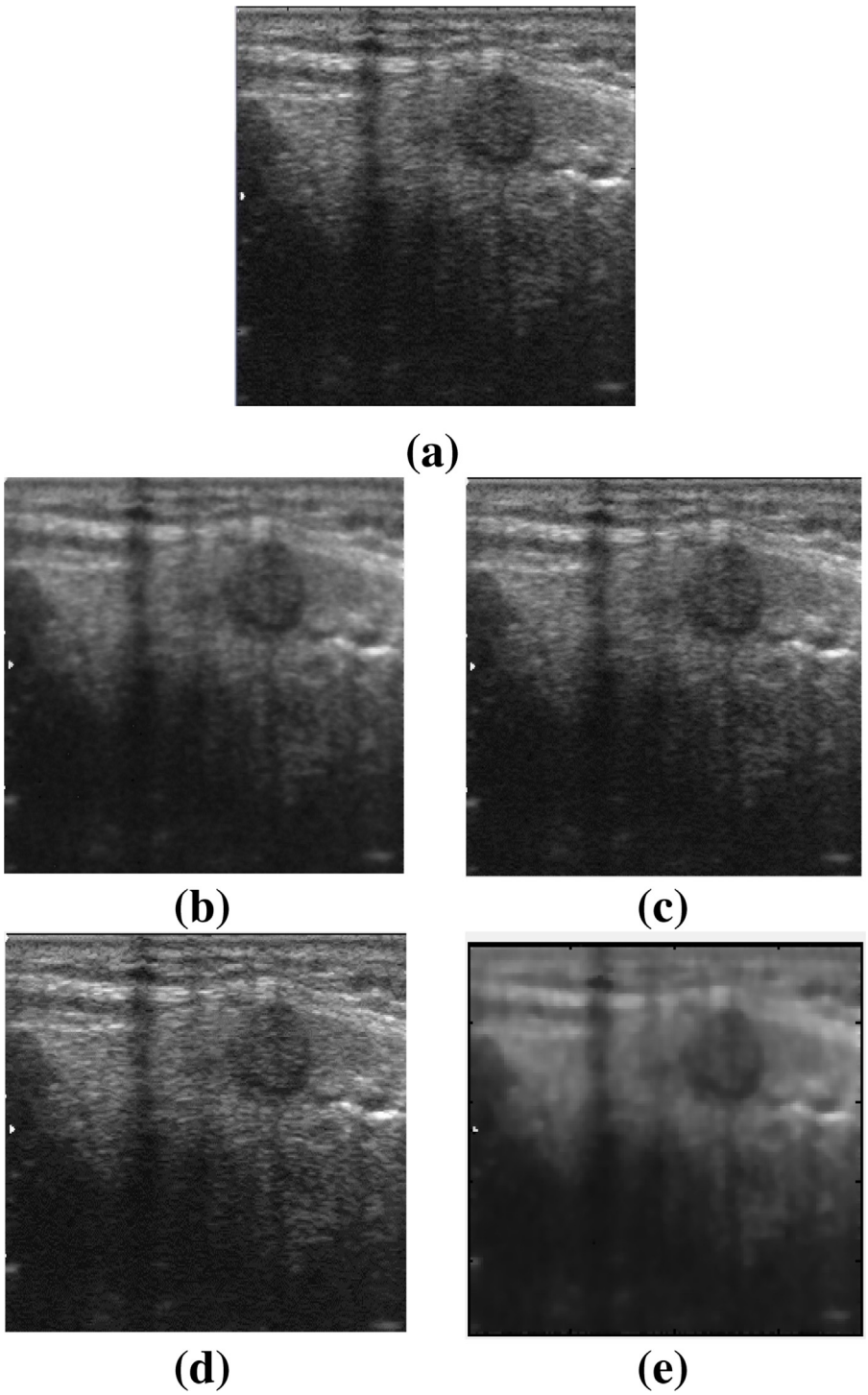

Fig. 8. Results on the thyroid ultrasound image (img9) **(a)** Original image. Denoised results on the image processed by **(b)** NRSNR **(c)** NTV **(d)** NNRSNR **(e)** NNTV.

4. Experimental results and discussion

4.1. Results on real thyroid ultrasound images

This section shows the experimental results of speckle reduction methods on real thyroid ultrasound images. The methods used for speckle reduction are NTV, NRSNR, NNRSNR and NNTV. Fig. 6(a) shows an original image. The result of NRSNR shown in Fig. 6(b) shows good speckle suppression but some spots and blurriness can be easily visualized.

The NTV method presented in Fig. 6(c) shows that the method has performed well both in terms of speckle suppression and edge preservation. From visual results shown in Fig. 6(d) and Fig. 6(e), it is observed that both the NNRSNR and the NNTV method in neutrosophic domain show better removal of speckle noise in homogeneous areas. Thus, it is concluded from the results that the methods in neutrosophic domain are performing better than the methods in spatial domain.

From Fig. 7, it has been observed that the NNTV can better preserved the nodule's boundaries in thyroid ultrasound image while the degree of speckle suppression is high as compared to NNRSNR

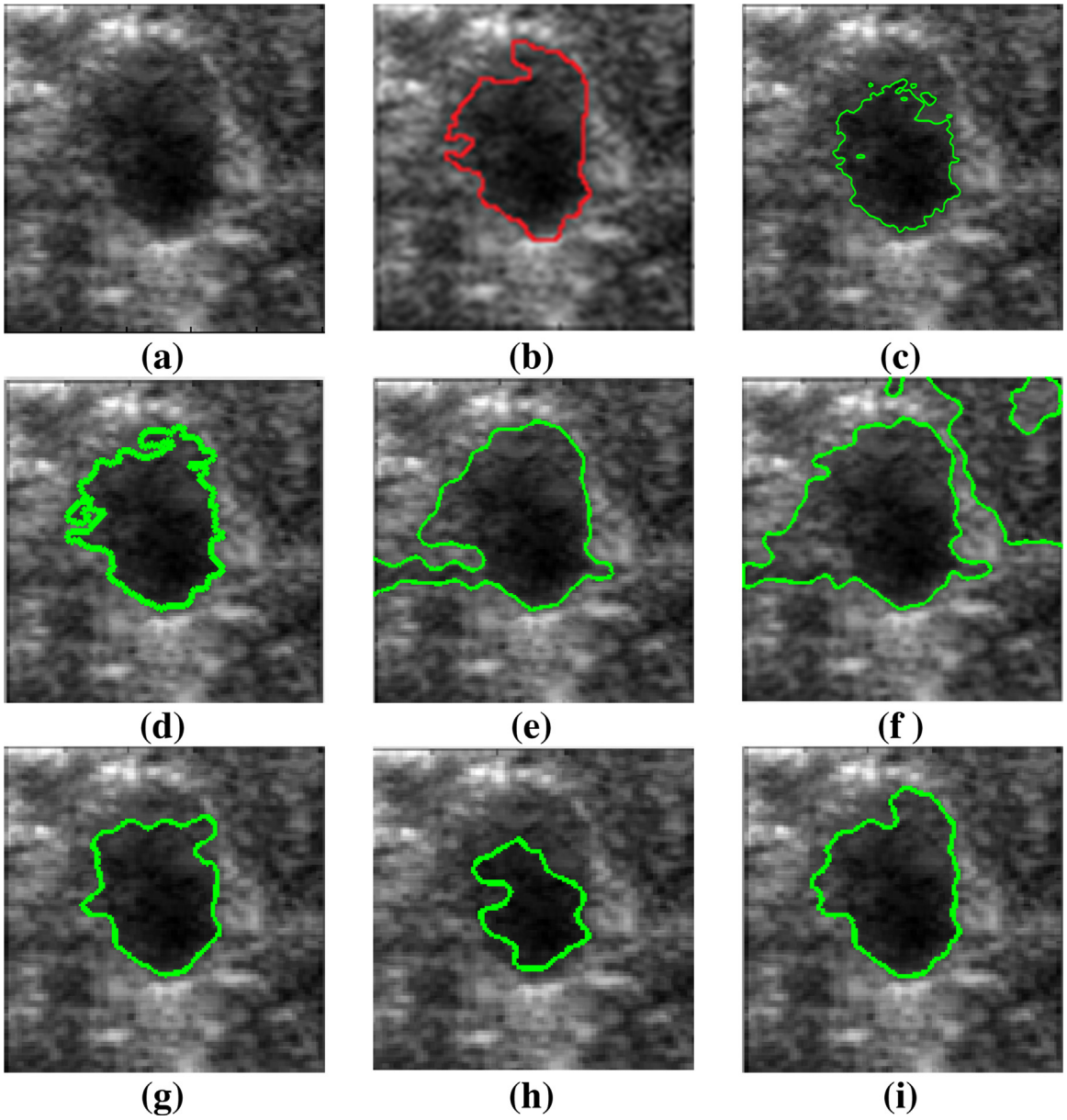

Fig. 9. **(a)** Ultrasound image (img23) **(b)** Ground Truth. Segmentation results by **(c)** DRLSE **(d)** NW **(e)** ACWE **(f)** FLSM **(g)** NCM **(h)** NLM **(i)** NDRLS.

as shown in Fig. 7(e). It has also been observed that the speckle is effectively removed and structure of thyroid nodule has been well preserved in neutrosophic domain by NNTV using Nakagami distribution statistics.

Fig. 8 also shows the visual results of NRSNR, NTV, NNRSNR and NNTV. The evaluation of both NRSNR and NNRSNR show that the neutrosophic domain improves the despeckling performance shown in Fig. 8(b) and Fig. 8(d). NNTV significantly removes the speckle noise both in textured and homogeneous areas. Further, it can be used for accurate segmentation and differentiation of distinct tissues as shown in Fig. 8(e). It is also noticed that NNTV can better preserved the nodule's boundaries in thyroid ultrasound image while the degree of speckle suppression is high as compared to NNRSNR method. It is also observed that the speckle is removed effectively and nodule structure has been well preserved in neutrosophic domain by NNTV using Nakagami distribution statistics as compared to NTV method given in Fig. 8(c).

4.2. Comparison of NDRLS with other segmentation methods

Further, the performance of segmentation methods in neutrosophic domain is compared with proposed method on dataset 1 and dataset 2 of thyroid ultrasound images. Table 1 and Table 2 lists the values of all quality metrics. As evident from results, it is observed that NDRLS outperforms all other neutrosophic domain methods by achieving high values in terms of TP, DC and OM. The larger values of area based metrics produced by NDRLS ensure more resemblance between the region segmented by segmentation methods [39]. The NDRLS also reveals an improvement in FP and HD as compared to other methods as listed in Table 1 and Table 2. Furthermore, smallest HD value specifies the superiority of proposed method as compared to other methods. The NDRLS is better than other methods in terms of FP, TP, OM, DC and HD. The results show that more overlapping area is obtained by NDRLS as compared to NCM [12] and NLM [39].

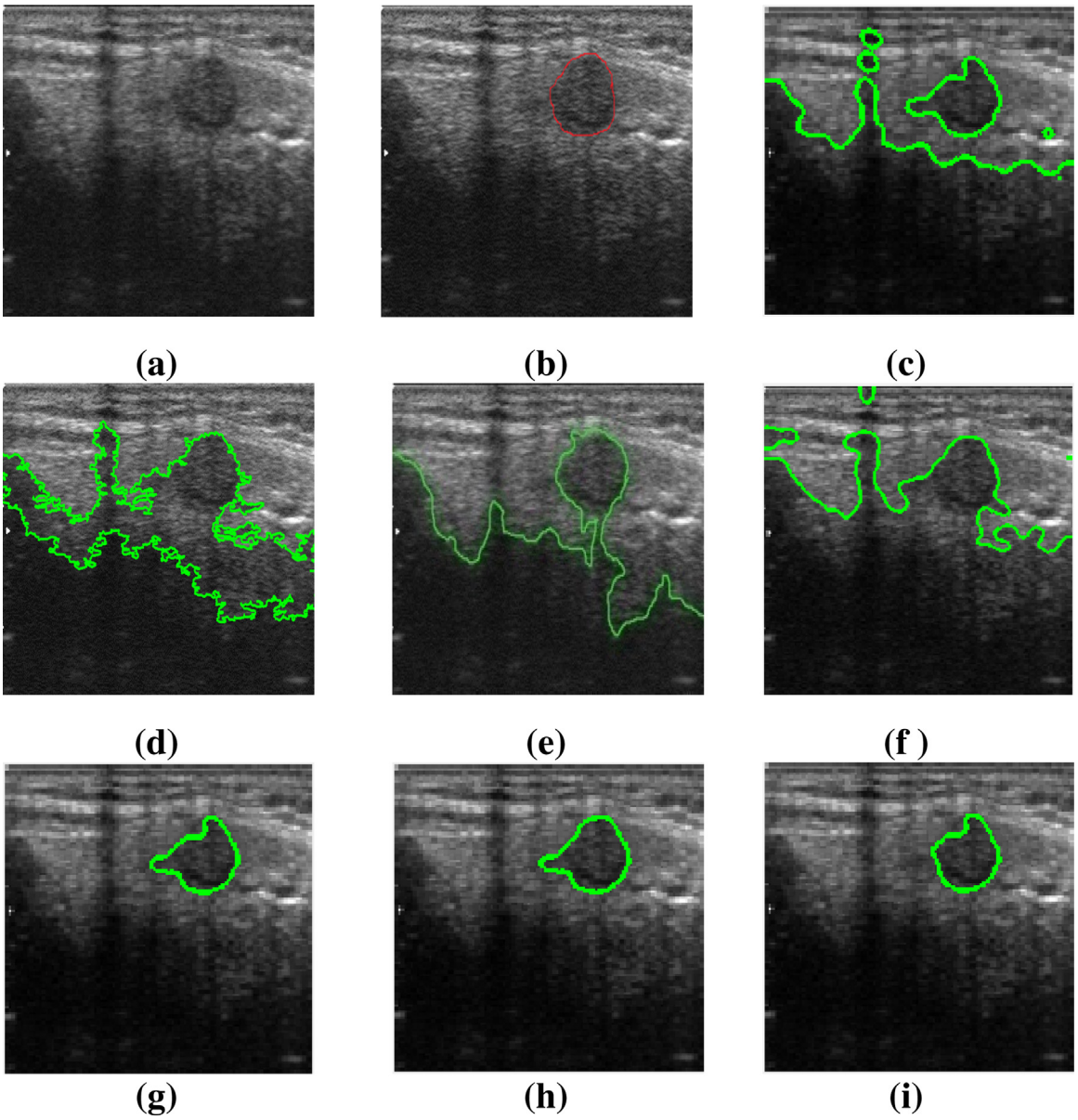

Fig. 10. Ultrasound image (img318) **(a)** Original image **(b)** Ground Truth. Segmentation results by **(c)** DRLSE with threshold **(d)** NW **(e)** ACWE **(f)** FLSM **(g)** NCM **(h)** NLM **(i)** NDRLS.

Table 1
Performance measures of segmentation methods on dataset 1.

Metrics Methods	TP (%)	FP (%)	DC (%)	OM (%)	HD (pixels)
NCM	90.07 ± 7.3	10.44 ± 5.2	91.55 ± 8.80	89.14 ± 10.0	0.66 ± 0.40
NLM	91.80 ± 6.2	9.90 ± 8.5	92.40 ± 4.0	90.10 ±n7.0	0.90 ± 0.08
NDRLS	93.45 ± 2.5	4.07 ± 4.8	93.8 ± 3.70	92.8 ± 4.6	0.24 ± 0.08

Table 2
Performance measures of segmentation methods on dataset 2.

Metrics Methods	TP (%)	FP (%)	DC (%)	OM (%)	HD (pixels)
NCM	88.5 ± 6.2	10.93 ±10.9	78.50 ± 18.4	78.44 ± 18.3	20.1 ± 19.7
NLM	89.0 ± 6.9	11.41 ± 13.3	89.00 ± 6.9	89.00 ± 6.9	4.3 ± 4.01
NDRLS	**95.92 ± 3.70**	**7.04 ± 4.21**	**93.88 ± 2.59**	**91.18 ± 7.04**	**0.52 ± 0.20**

Table 3
Comparison of NLM with NDRLS on dataset 2.

Metrics Methods	TP(%)	FP(%)	OM(%)	DC(%)	MAD(pixels)	HD (pixels)
NLM	92.3 ± 4.9	8.4 ± 4.9	91.9 ± 5.1	94.5 ±2.7	1.9 ± 1.2	0.9 ± 0.08
NDRLS	95.4 ± 3.5	7.3 ± 5.3	93.1 ± 5.2	94.2 ±4.6	0.2 ± 0.9	0.2 ± 0.82
***p*-value**	<0.005	<0.005	<0.005	<0.005	3.3×10^{-3}	1.9×10^{-9}

Table 4
Performance of NDRLS with speckle reduction or without speckle reduction on dataset 2.

Metrics Method	TP (%)	FP (%)	OM (%)	DC (%)	MAD (pixels)	HD (pixels)
Without speckle reduction	94.9 ± 3.1	7.3 ± 5.3	92.9 ± 4.9	93.9 ± 0.4	0.2 ± 0.8	0.2 ± 0.72
With speckle reduction	95.4 ± 3.5	7.1 ± 4.9	93.1 ± 5.2	94.2 ± 4.6	0.2 ± 0.9	0.2 ± 0.81
p-value	<0.05	<0.05	<0.05	<0.05	<0.05	<0.05

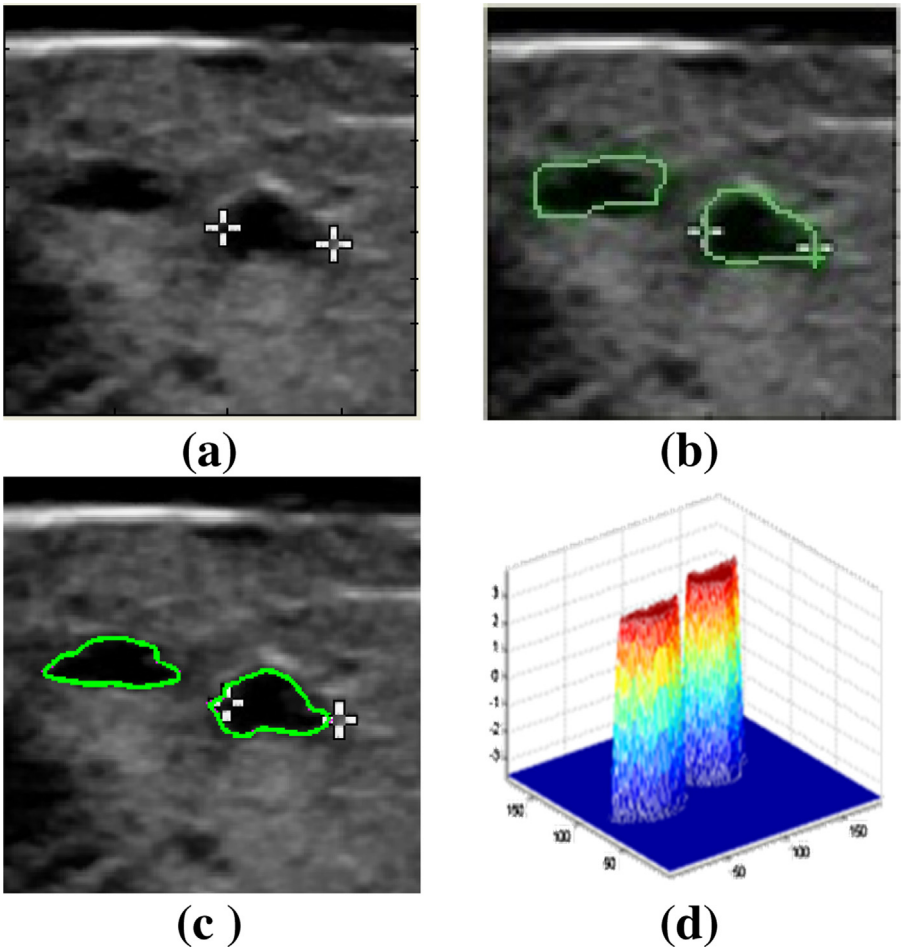

Fig. 11. **(a)** Original image (img32) Dataset 1 **(b)** Ground Truth. Segmentation result by **(c)** NDRLS **(d)** Corresponding 3D Level Set mesh.

The quantitative results of proposed method are also supplemented with subjective outcomes. Two real thyroid ultrasound images from dataset 2 are illustrated in Fig. 9 and Fig. 10 respectively. Both images have low contrast with weak boundaries between nodules and adjoining tissues. Fig. 9 shows the visual comparison of NDRLS with all aforementioned methods. Fig. 9 (a) illustrates the original thyroid ultrasound image and Fig. 10(b) shows the ground truth image. The image segmented by DRLSE is affected as the region can be easily trapped into inappropriate local minima due to local change of intensities as illustrated in Fig. 10(c). It is observed that the images segmented by Neutrosophic Watershed (NW) [44–46] Active Contour without Edges (ACWE) [5] and Fuzzy Level Set Method (FLSM) [28] are susceptible to noise and the contour can pass through weak edges as shown in Fig. 9(d), Fig. 9(e) and Fig. 9(f) respectively. In addition, Fig. 9(g) illustrates the visual outcome of NCM, which shows that the boundary of segmented nodule is not close to the boundary marked by an expert. As evident from Fig. 9(h), NLM method is not able to segment the entire nodule properly. From results, it is found that segmented nodules by NDRLS are very close to the manual segmentation as shown in Fig. 9(i). The proposed method can handle pixels uncertainty, fuzziness and indeterminacy.

Fig. 10(a) shows the original ultrasound image and Fig. 10(b) illustrates the ground truth image. The image segmented by DRLSE is able to attain delineate nodule regions with non-nodule regions also as shown in Fig. 10(c). While from Fig. 10(d), Fig. 10(e) and Fig. 10(f), it is apparent that the nodule is not accurately segmented out because of weak boundaries and poor contrast. The NCM and NLM are able to segment the nodule in neutrosophic domain but the obtained boundary is not much closer to the ground truth boundary as illustrated in Fig. 10(g) and Fig. 10(h). The best segmentation of nodule is achieved by NDRLS as the attained segmentations are very smooth and completely adapted to the thyroid nodule boundaries as shown in Fig. 10(i).

Additionally, NDRLS can prevent leakage through weak edges resulting in accurate extraction of nodule boundaries by handling the intensity in-homogeneity well. The comparison of NDRLS and NLM are given in Table 2. The mean values of TP, DC and OM obtained with NDRLS are 95.4%, 94.2% and 93.1% respectively. Mostly, NDRLS converge to higher values than NLM. The mean difference values of OM, DC, TP and MAD obtained by the NLM and

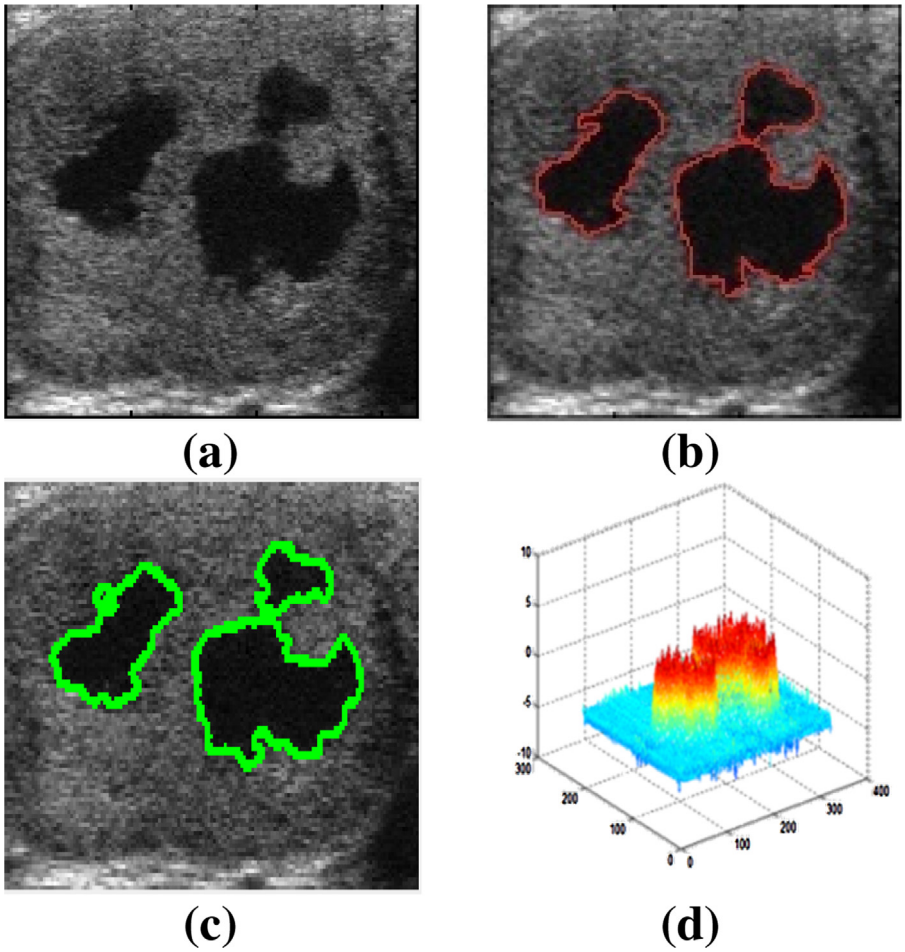

Fig. 12. **(a)** Original image (img40) Dataset 2 **(b)** Ground truth. Segmentation results by **(c)** NDRLS **(d)** Corresponding 3D Level Set mesh.

NDRLS methods are $1.2 \pm 0.1, 2.97 \pm 2.5, 3.1 \pm 1.4$ and 1.7 ± 0.3 pixel respectively, in support of NDRLS. Also, Table 3 demonstrates the statistical significant difference between NLM and NDRLS to show that their application is viable in medical practice. The statistical significance of this result is validated by p-value. The resulting p-value of each metric is significant in a 0.005 level. Further, the experiments were carried out for the segmentation of nodules with or without speckle reduction to evaluate the robustness of NDRLS in presence of artifacts. Table 3 listed the results of various evaluation metrics with p-value and standard deviation. If p-value is less than 0.01, and then the difference is considered as highly significant, in statistics. If p-value is between 0.01 and 0.05, and then the difference is considered as significant. The resulting p-value of each metric is significant in a 0.05 level. The variation in TP rate from 95.4% to 94.9% shows that NDRLS with speckle reduction covers slightly more region than without speckle reduction. The FP rate from 7.3% to 7.1% also indicates less difference between both methods in mis-coverage of the non-nodule regions.

The p-values of OM and DC are also less than 0.05, which indicate significant difference. The differences between the evaluation results of NDRLS with or without speckle reduction are significant. The performance of NDRLS with or without speckle reduction is also demonstrated by the boundary error metrics too, which show that the contours generated by NDRLS with or without speckle reduction are much closer to the manual delineations as given in Table 4. As evident from these results, it is observed that NDRLS can be applied without speckle reduction for the nodule segmentation. All these results justify the good indeterminacy handling capability of neutrosophic domain.

Further, two images from different datasets are selected to demonstrate the capability of NDRLS in delineating multiple nodules as illustrated in Fig. 11 and Fig. 12. The original thyroid ultrasound image consisting of multiple nodules is shown in Fig. 11(a) and Fig. 12(a) whereas Fig. 11(b) and Fig. 12(b) illustrate the ground truth image. Fig. 11(c) and Fig. 12(c) illustrate that the NDRLS can segment multiple nodules with its 3D level set mesh shown in Fig. 11(d) and Fig. 12(d).

5. Conclusion and discussion

Neutrosophy is an important tool for removing uncertainty from ultrasound images and is most widely used in image denoising. In this work, an automated CADe system for the segmentation of nodules in thyroid ultrasound images has been developed. A Neutrosophic domain Nakagami Total Variation method has been used for speckle reduction and Neutrosophic based Distance Regularized Level Set method is proposed for automated segmentation of thyroid nodules in ultrasound images. The experimental results show that the initial contours are automatically identified very near to the actual nodule boundaries of the thyroid gland which can be fastly refined by level set. In experiments, NDRLS is found to be highly efficient, robust and accurate. The NDRLS automatically approximates the optimal parameters from NLM and becomes stable as the implicit interface comes closer to the desired contours. The experimental results reveal that the NDRLS performed better than other methods in handling indeterminacy and in-homogeneity. The NDRLS can separate all nodules in spite of blurry and unclear edges.

It can also prevent boundary leakage into adjoining tissues and can smooth vague background. Besides the above benefits, NDRLS can also segment multiple nodules. Additionally, NDRLS does not need any training and input from the user. Furthermore, the method is capable of revealing thyroid nodule boundaries in spite of intensity variations. The higher values of quality metrics achieved by the NDRLS method over other state-of-art methods, recommends its application in medical practice. Finally, a fully automated CADe system for the segmentation of nodules in thyroid ultrasound images has been developed with graphical user interface without any human intervention. It may be used as a second opinion tool to assist endocrinologists for automated and accurate delineation of thyroid nodules in ultrasound images. This helps to reduce the number of false positives and improves the accurate detection of thyroid nodules.

This research work successfully solved the computer-aided detection problems by systematically developing speckle reduction, automatic ROI extraction and segmentation methods that can improved the quality of ultrasound images and aid doctors in detecting the thyroid nodules. This work would definitely be an aid for future research as it provides techniques for speckle suppression and accurate detection of thyroid nodules in ultrasound images for an effective diagnosis. Additionally, the proposed detection system is fully automatic and requires no training but still there are many aspects need to be studied in the future in order to achieve better performance and accuracy. The present work suggests few directions and challenges for the researchers to further explore the area of thyroid ultrasound image processing and analysis in detail. In future, the work can be extended for the delineation of isoechoic thyroid nodules. As this research work has focused only on the development of CADe system for the segmentation of nodule from thyroid ultrasound images. The texture features and classification techniques can be combined to develop Computer-Aided Diagnosis (CADx) system with the proposed fully automatic CADe system, which will be more useful for thyroid nodule diagnosis. Furthermore, research utilizing larger datasets of real-time images with feedback information is required to validate the benefits of NDRLS on other tissues. The method is general and can be applied to other ultrasound images of diverse anatomical structures.

The further research can be extended to validate the proposed system to three dimensional ultrasound images and Doppler ultrasound images as this work only deal with B-mode ultrasound images. Other imaging modalities are still need to be explored with this system. Neutrosophy based techniques can be applied to other image processing problems such as image retrieval. Neutrosophic domain methods can be compared to wavelets to show their effectiveness over other domains.

References

[1] K. Ain, M.S. Rosenthal, The Complete Thyroid Book, McGraw Hill Professional, 2010.
[2] U.R. Acharya, P. Chowriappa, H. Fujita, S. Bhat, S. Dua, J.E. Koh, K.H. Ng, Thyroid lesion classification in 242 patient population using gabor transform features from high resolution ultrasound images, Knowledge-Based Syst. (2016).
[3] S.J. Attia, Cytological detection of thyroid cancer by optical image analysis, J. Nat. Sci. Res. 5 (18) (2015) 57–60.
[4] S. Aja-Fernández, A.H. Curiale, G. Vegas-Sánchez-Ferrero, A local fuzzy thresholding methodology for multiregion image segmentation, Knowlegde Based Syst. 83 (2015) 1–12.
[5] T.F. Chan, L.A. Vese, Active contours without edges, IEEE Trans. Image Process. 10 (2) (2001) 266–277.
[6] R.F. Chang, W.J. Wu, W.K. Moon, D.R. Chen, Automatic ultrasound segmentation and morphology based diagnosis of solid breast tumors, Breast Cancer Res. Treat. 89 (2) (2005) 179–185.
[7] K.S. Chuang, H.L. Tzeng, S. Chen, J. Wu, T.J. Chen, Fuzzy c-means clustering with spatial information for image segmentation, Comput. Med. Imaging Graph. 30 (1) (2006) 9–15.
[8] Y. Guo, H.D. Cheng, New neutrosophic approach to image segmentation, Pattern Recogn. 42 (5) (2009) 587–595.
[9] Y. Guo, H.D. Cheng, Y. Zhang, A new neutrosophic approach to image denoising, New Math. Nat. Comput. 5 (03) (2009) 653–662.
[10] Y. Guo, H.D. Cheng, J. Tian, Y. Zhang, A novel approach to speckle reduction in ultrasound imaging, Ultrasound Med. Biol. 35 (4) (2009) 628–640.
[11] Y. Guo, C. Zhou, H. Chan, A. Chughtai, J. Wei, L.M. Hadjiiski, E.A. Kazerooni, Automated iterative neutrosophic lung segmentation for image analysis in thoracic computed tomography, Med. Phys. 40 (8) (2013) 1–11.
[12] Y. Guo, A. Sengur, NCM: Neutrosophic c-means clustering algorithm, Pattern Recogn. 48 (8) (2015) 2710–2724.
[13] Y. Han, X. Feng, G. Baciu, W. Wang, Nonconvex sparse regularizer based speckle noise removal, Pattern Recogn. 46 (3) (2013) 989–1001.
[14] V.P. Kharchenko, P.M. Kotlyarov, M.S. Mogutov, Y.K. Alexandrov, A.N. Sencha, Y.N. Patrunov, D.V. Belyaev, Ultrasound diagnostics of thyroid diseases, Springer Sci. Bus. Media. (2010).
[15] A. Keerthivasan, J.J. Babu, G.F. Sudha, Speckle noise reduction in ultrasound images using fuzzy logic based on histogram and directional differences, In Communications and Signal Processing (ICCSP), 2013 International Conference on IEEE (2013) 499–503.
[16] E.G. Keramidas, D. Maroulis, D.K. Iakovidis, TND: a thyroid nodule detection system for analysis of ultrasound images and videos, J. Med. Syst. 36 (3) (2012) 1271–1281.
[17] B. Kavitha, S. Karthikeyan, P.S. Maybell, An ensemble design of intrusion detection system for handling uncertainty using Neutrosophic Logic Classifier, Knowledge-Based Syst. 28 (2012) 88–96.
[18] E. Karabatak, Y. Guo, A. Sengur, Modified neutrosophic approach to color image segmentation, J. Electron. Imaging 22 (1) (2013), 013005–013005.
[19] D. Koundal, S. Gupta, S. Singh, Computer-aided diagnosis of thyroid nodule: a review, Int. J. Comput. Sci. Eng. Surv. 3 (4) (2012) 67.
[20] D. Koundal, S. Gupta, S. Singh, Applications of neutrosophic and intuitionistic fuzzy set on image processing, in: National Conference on Green Technologies: Smart and Efficient Management (GTSEM-2012), SLIET, Longowal, 2012, pp. 1–4.
[21] D. Koundal, S. Gupta, S. Singh, Speckle reduction filter in neutrosophic domain, In Proceedings of International Conference of Biomedical Engineering and Assisted Technologies (2012) 786–790.
[22] D. Koundal, S. Gupta, S. Singh, Survey of computer-aided diagnosis of thyroid nodules in medical ultrasound images, in: In Advances in Computing and Information Technology, Springer, Berlin Heidelberg, 2013, pp. 459–467.
[23] D. Koundal, S. Gupta, S. Singh, Nakagami-based total variation method for speckle reduction in thyroid ultrasound images, Proc. Inst. Mech. Eng. Part H: J. Eng. Med. (2015) (0954411915621340).
[24] D. Koundal, R. Vishraj, S. Gupta, S. Singh, An automatic ROI extraction technique for Thyroid Ultrasound image, In 2015 2nd International Conference on Recent Advances in Engineering & Computational Sciences (RAECS) IEEE (2015) 1–5.
[25] D. Koundal, S. Gupta, S. Singh, Speckle reduction method for thyroid ultrasound images in neutrosophic domain, IET Image Proc. 10 (2) (2016) 167–175.
[26] D. Koundal, Automated System for Delineation of Thyroid Nodules in Ultrasound Images, Doctoral dissertation, Panjab University, Chandigarh, India, 2016.
[27] C. Li, C. Xu, C. Gui, M.D. Fox, Distance regularized level set evolution and its application to image segmentation, IEEE Trans. Image Process. 19 (12) (2010) 3243–3254.
[28] B.N. Li, C.K. Chui, S. Chang, S.H. Ong, Integrating spatial fuzzy clustering with level set methods for automated medical image segmentation, Comput. Biol. Med. 41 (1) (2011) 1–10.
[29] Y.H. Lee, D.W. Kim, H.S. In, J.S. Park, S.H. Kim, J.W. Eom, M.H. Rho, Differentiation between benign and malignant solid thyroid nodules using an US classification system, Korean J. Radiol. 12 (5) (2011) 559–567.
[30] A.S. McQueen, K.S. Bhatia, Thyroid nodule ultrasound: technical advances and future horizons, Insights Imaging 6 (2) (2015) 173–188.
[31] J. Mohan, V. Krishnaveni, Y. Guo, A neutrosophic approach of MRI denoising, In Image Information Processing (ICIIP), International Conference on IEEE (2011) 1–6.
[32] J. Mohan, V. Krishnaveni, Y. Guo, MRI denoising using nonlocal neutrosophic set approach of Wiener filtering, Biomed. Signal Process. Control 8 (6) (2013) 779–791.
[33] J. Mohan, V. Krishnaveni, Y. Guo, A new neutrosophic approach of Wiener filtering for MRI denoising, Measure. Sci. Rev. 13 (4) (2013) 177–186.
[34] B. Moifo, E.O. Takoeta, J. Tambe, F. Blanc, J.G. Fotsin, Reliability of thyroid imaging reporting and data system (TIRADS) classification in differentiating benign from malignant thyroid nodules, Open J. Radiol. 3 (03) (2013) 103.
[35] S. Osher, J.A. Sethian, Fronts propagating with curvature-dependent speed: algorithms based on Hamilton-Jacobi formulations, J. Comput. Phys. 79 (1) (1988) 12–49.
[36] L. Pedraza, C. Vargas, F. Narváez, O. Durán, E. Muñoz, E. Romero, An open access thyroid ultrasound image database, in: In Tenth International Symposium on Medical Information Processing and Analysis. International Society for Optics and Photonics, (2015, January), 2015, p. 92870W.
[37] M.A. Savelonas, D.K. Iakovidis, N. Dimitropoulos, D. Maroulis, Computational characterization of thyroid tissue in the radon domain, In Twentieth IEEE International Symposium on Computer-Based Medical Systems (CBMS'07) IEEE (2007) 189–192.
[38] A.A. Salama, F. Smarandache, M. Eisa, Introduction to image processing via neutrosophic techniques, Neutrosophic Sets Syst. 5 (2014) 59–64.

[39] J. Shan, H.D. Cheng, Y. Wang, A novel segmentation method for breast ultrasound images based on neutrosophic l-means clustering, Med. Phys. 39 (9) (2012) 5669–5682.
[40] F. Smarandache, A Unifying Field in Logics: Neutrosophic Logic. Neutrosophy, Neutrosophic Set, Neutrosophic Probability: Neutrsophic Logic. Neutrosophy, Neutrosophic Set, Neutrosophic Probability. Infinite Study, 2005.
[41] F. Smarandache, Indeterminate masses, elements and models in information fusion, Int. J. Adv. Mechatronic Syst. 5 (6) (2013) 365–372.
[42] Thyro, http://www.seer.cancer.gov/thyro.htm, 2016.
[43] Y. Zhang, R. Sankar, W. Qian, Boundary delineation in transrectal ultrasound image for prostate cancer, Comput. Biol. Med. 37 (11) (2007) 1591–1599.
[44] M. Zhang, L. Zhang, H.D. Cheng, A neutrosophic approach to image segmentation based on watershed method, Signal Process. 90 (5) (2010) 1510–1517.
[45] Y. Zhang, H.D. Cheng, J. Tian, J. Huang, X. Tang, Fractional subpixel diffusion and fuzzy logic approach for ultrasound speckle reduction, Pattern Recogn. 43 (8) (2010) 2962–2970.
[46] M. Zhang, L. Zhang, H.D. Cheng, Segmentation of ultrasound breast images based on a neutrosophic method, Opt. Eng. 49 (11) (2010), 117001–117001.